International Journal of Engineering Technology Science and Research
IJETSR
www.ijetsr.com
ISSN 2394 – 3386
Volume 5, Issue 4
April 2018

Influence of Ni^{2+} Ion Substitution on Structural and Magnetic Properties of Copper Ferrite Nanoparticles

Sonia Gaba
Department of Physics, DCR University of Sci. & Techn., Murthal, Sonepat, Haryana, India
Ashok Kumar
Department of Physics, DCR University of Sci. & Techn., Murthal, Sonepat, Haryana, India
Pawan S Rana
Department of Physics, DCR University of Sci. & Techn., Murthal, Sonepat, Haryana, India

ABSTRACT

Nickel doped copper ferrite nanoparticles $Ni_xCu_{1-x}Fe_2O_4$ (x= 0.2, 0.4, 0.6, and 0.8) have been synthesized by sol-gel technique.The synthesized samples were characterized by various analytical techniques like powder X-ray diffractometer (XRD), scanning electron microscope (SEM), transmission electron microscope (TEM), Fourier transform infrared spectroscopy (FTIR) and vibrating sample magnetometer (VSM). XRD patterns of synthesized samples show the single phase formation of spinel crystalline structure without any trace of impurity. The crystallite size decreases with the increase in Ni ion concentración. FTIR analysis confirms the substitution of Ni^{2+} ions resulted from the migration of Fe^{2+} ions at octahedral to tetrahedral sites. SEM images shows that almost all the particles are spherical in shape. The particle sizes obtained from TEM micrographs are in agreement with crystallite size calculated from XRD results. The M-H loops indicate that saturation magnetization increases with increasing nickel ion content. The enrichment in the magnetic properties of the $Ni_xCu_{1-x}Fe_2O_4$ nanopowder indicates that these materials are suitable candidate as magnetic catalyst.

Keywords: Ferrites; Spinel Structure; Sol-Gel; Crystallite Size; Magnetisation

1. INTRODUCTION

Magnetic nanoparticles have been studied extensively in recent years and these ferrites form an important class of materials due to their unique magnetic and electric properties [1]. The ferrite nanoparticles exhibit interesting and substantially different magnetic properties than those of bulk materials due to their large surface to volume ratio. These magnetic particles have been widely used in different areas such as in magnetic media, electronic devices, gas sensors, information storage system, drug delivery, microwave absorbent, catalyst, hyperthermia, magnetic resonance imaging, ferrofluids, lithium-ion batteries, magnetic diagnostics, high frequency applications etc. [2-6]. The ferrite nanoparticles have spinel structure (AB_2O_4) which consists of two sites, the tetrahedral A-site and octahedral B-site. The substitution of various magnetic and nonmagnetic ions at the A site and B site markedly influences the properties of the ferrites. The large variations in physical properties have been attributed to the ability of metal ions to accommodate and their distribution on the available sites. Nickel copper ferrites are soft spinel ferrites being used in multilayer chip inductor applications due to their high electrical resistivity, chemical stability and exceptional magnetic properties at high frequencies [7]. It is well known that the physical properties of the spinel ferrites are very sensitive to the method of preparation. The selection of an appropriate synthesis method is a key to obtain good quality ferrite nanoparticles [8]. Several methods such as chemical co-precipitation, sol-gel, ball milling, citrate precursor, mechanochemical, glycine nitrate, modified oxidation, hydrothermal, solid state etc. are reported in the literature [9-12] for the synthesis of nickel copper mixed ferrite nanoparticles. Recently the

International Journal of Engineering Technology Science and Research
IJETSR
www.ijetsr.com
ISSN 2394 – 3386
Volume 5, Issue 4
April 2018

efficient cost effective sol-gel method [13] has been used to synthesize ultrafine nanomagnetic particles. This method has advantageous over another synthesis technique as it is simple and fast process with better control of desired stoichiometry. In our present work Ni doped copper ferrite nanoparticles with composition $Ni_xCu_{1-x}Fe_2O_4$ (x= 0.2, 0.4, 0.6 and 0.8) have been synthesized using sol-gel method. The influence of nickel ion substitution on the structural and magnetic properties of copper ferrite nanoparticles has been explored.

2. EXPERIMENTAL

2.1 SAMPLE PREPARATION

Nanocrystalline $Ni_xCu_{1-x}Fe_2O_4$ (x = 0.2, 0.4, 0.6 and 0.8) ferrite particles have been synthesized using sol-gel technique. In this method, Sigma Aldrich analytical grade salts of Ni $(NO_3)_2{\cdot}6H_2O$ (99.9% purity), Cu $(NO_3)_2.6H_2O$ (99.9% purity) and Fe $(NO_3)_3{\cdot}9H_2O$ (99.9% purity) were taken as the starting materials without further purification. Homogeneous solutions were obtained by dissolving stoichiometric ratios of these salts in adequate amount of ethylene glycol at room temperature. These solutions were then mixed together under continuous stirring and heating till the formation of sol. The sol was then heated at 60 °C with constant stirring to form a wet gel. The gel was then dried overnight at 150 °C in temperature controlled oven to obtain ferrite nanopowder. The powder was further grounded for about an hour and was used for further characterizations.

2.2 Characterization Techniques

The structural characterization of Ni substituted copper ferrite nanoparticles were performed using Rigaku make powder X-ray diffractometer at 40kV and 30mA, with Cu Kα (λ=1.54059Å) radiation. The scanning was done in the 2θ range from 20° to 70° with step size of 0.02°/s. SEM images were recorded by using ZEISS EVO MA10 SEM scanning electron microscope. The morphology and shape of synthesized nanoparticles were studied with the help of transmission electron microscope (TEM) model Hitachi (H-7500). The Fourier transform infrared (FTIR) spectrum of as synthesized samples were recorded with a NICOLET 5700 FTIR spectrometer in the range 400 – 4000 cm^{-1} at room temperature using KBr technique. The powdered samples were mixed with KBr matrix and then dry pressed using a pelletizer at 100MPa to form pellets. All spectrums have been recorded in the transmission mode. Magnetic measurements i.e. M-H loops of the synthesized particles have been studied at room temperature using a vibrating sample magnetometer model ADE-EV9, Make Microsense.

3. RESULTS AND DISCUSSIONS

3.1 XRD Analysis

X–ray diffraction patterns of as synthesized $Ni_xCu_{1-x}Fe_2O_4$ for x= 0.2, 0.4, 0.6, 0.8, samples are shown in Fig.1. XRD patterns of all the samples exhibit all major peaks related to spinel crystalline structure indicating the ultrafine nature of the particles and are in well agreement with the JCPDs card no. 086-2287 .To calculate the crystallite size, a slow scan of intense diffraction peaks (220), (311), (400), (422), (511) and (400) was recorded. From the full width at half maximum (FWHM) of peaks, the crystallite size was calculated using the Scherer's formula [14].

$$D = \frac{k^{a}}{{}_{hkl}\cos^{-}} \qquad (1)$$

where k is a Scherer constant (0.89), D is crystallite size in nm, β is full width at half maxima measured in radians, θ is the Bragg's angle corresponding to a peak and λ is wavelength of X-rays (1.5406 Å) used. In a cubic spinel structure, the size of the unit cell (lattice constant, a) was calculated by using the relation

International Journal of Engineering Technology Science and Research
IJETSR
www.ijetsr.com
ISSN 2394 – 3386
Volume 5, Issue 4
April 2018

$$a = d\sqrt{h^2 + k^2 + l^2} \qquad (2)$$

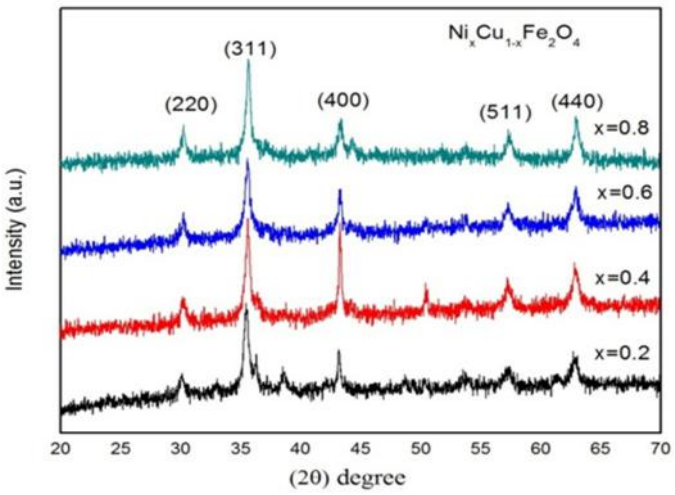

Fig.1: X-ray diffraction pattern of $Ni_xCu_{1-x}Fe_2O_4$ (x=0.2, 0.4, 0.6, 0.8) samples.

X-ray density (ρ_x) is calculated by using the relation [15]:

$$\rho_x = \frac{8M}{NV} \qquad (3)$$

Where M is molecular weight of sample, N is Avogadro's no. and $\mathbf{V=a^3}$

Measured density is calculated by the relation [15]:

$$\rho = \frac{m}{\pi r^2 h} \qquad (4)$$

Where m is mass, r is radius and h is height for cylindrical pellets of the sample.

Porosity (P) of sample is determined using the relation [15]:

$$P = 1 - \frac{\rho}{\rho_x} \qquad (5)$$

Ionic radii (r_A and r_B) on A- site and B- site of all the samples were calculated by using the relations [16]:

$$r_A = \left(\mu - \frac{1}{4}\right) a\sqrt{3} - R_o \qquad (6)$$

$$r_B = \left(\frac{5}{8} - \mu\right) a - R_o \qquad (7)$$

Where μ is oxygen ion parameter (0.381Å), R_o is the radius of oxygen ion (1.32Å).

International Journal of Engineering Technology Science and Research
IJETSR
www.ijetsr.com
ISSN 2394 – 3386
Volume 5, Issue 4
April 2018

Jump length of A-site (L_A) and B-site (L_B) can be calculated using [16]:

$$L_A = \frac{a\sqrt{3}}{4} \quad (8)$$

$$L_B = \frac{a\sqrt{2}}{4} \quad (9)$$

All the structural parameters calculated from the XRD diffraction pattern are listed in Table 1. As shown in Fig.2, the crystallite size and the lattice parameter decreases with increasing Ni^{2+} ion concentration which may be due to the smaller ionic radii of Ni^{2+} ions (0.69Å) ions as compared to Cu^{2+} ions (0.73Å). The porosity also decreases with increasing nickel ion concentration. This variation is attributed to the atomic weight and density of the nickel ion (53.933, 8.91 gm/cm^3) which is smaller than that of copper ion (63.546, 8.96 gm/cm^3). It can be clearly seen from the Table 1 that r_A, r_B, L_A and L_B decreases with increasing Ni^{2+} content which is attributed to the substitution of smaller nickel ion as compared to copper ion at the octahedral site.

Table 1: Structural parameters of $Ni_xCu_{1-x}Fe_2O_4$ (x= 0.2, 0.4, 0.6, 0.8) samples.

Composition	d (Å)	D(nm)	a (Å)	$°_x$ (gm/cm^3)	$°_m$ (gm/cm^3)	Porosity P	r_A (Å)	r_B (Å)	L_A(Å)	L_B(Å)	Magnetization Ms (emu/gm)
$Ni_{0.2}Cu_{0.8}Fe_2O_4$	2.530	18	8.393	5.392	3.887	0.5161	0.4985	0.7782	3.6341	2.9661	17.18
$Ni_{0.4}Cu_{0.6}Fe_2O_4$	2.524	17	8.357	5.388	3.848	0.5143	0.4907	0.7692	3.6185	2.9541	28.69
$Ni_{0.6}Cu_{0.4}Fe_2O_4$	2.519	16	8.355	5.382	3.765	0.5137	0.4903	0.7687	3.6177	2.9534	33.07
$Ni_{0.8}Cu_{0.2}Fe_2O_4$	2.518	14	8.352	5.365	3.552	0.5111	0.4896	0.7680	3.6164	2.9524	39.98

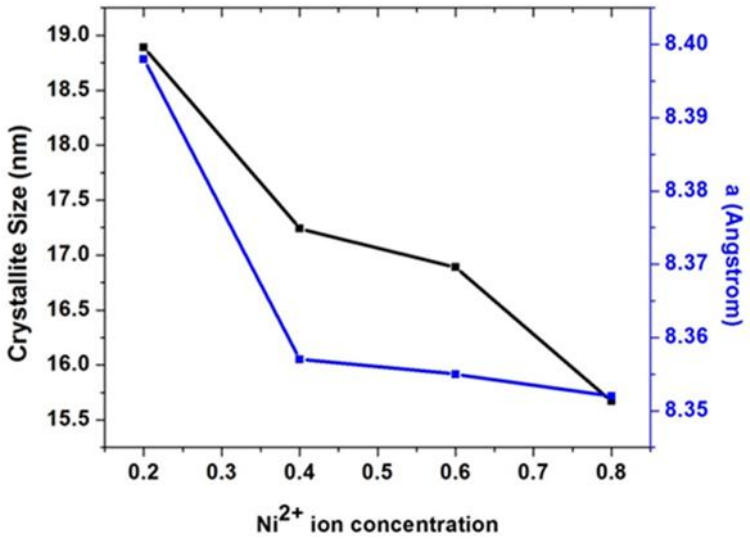

Fig.2: Variation of crystallite size and lattice parameter with Ni^{2+} concentration

International Journal of Engineering Technology Science and Research
IJETSR
www.ijetsr.com
ISSN 2394 – 3386
Volume 5, Issue 4
April 2018

3.2 FTIR Analysis

The FTIR spectra of investigated composition $Ni_xCu_{1-x}Fe_2O_4$ (x= 0.2, 0.4, 0.6 and 0.8) was recorded in the range of 400-4000 cm^{-1} is shown in fig.3. The infrared transmittance spectra of the prepared samples have been investigated to draw information about the structure and types of bonds present in the sample. In mixed ferrites, two main broad metal-oxygen bands are observed in the FTIR spectra and are designated as tetrahedral (A-site) and octahedral (B-site). The highest band v_1 corresponds to the intrinsic stretching vibrations of the metal and oxygen atoms at the tetrahedral site (M_{tetra}- O) and is generally observed in the range of 550-600 cm^{-1} while the lowest band v_2 corresponds to the stretching vibrations of the metal at the octahedral site (M_{octa} - O) [17] and observed around 490 cm^{-1}. On increasing Ni^{2+} ions content the absorption band v_1 increases linearly. The shift in v_1 band to the higher frequency is discussed in terms of the change in force constant, $F=4\pi^2c^2v^2\mu$ [18] where μ is reduced mass, ν is frequency in cm^{-1} & c is velocity of light (Reduced mass can be found as: $\mu=m_1m_2/(m_1+m_2)$ where m_1 & m_2 are atomic weight of metals). Hence the octahedral sites are completely occupied by nickel ions and with increasing content of Ni $^{2+}$ ions, the Fe^{3+} are forced at tetrahedral sites to replace copper ions. While going from one composition to another, the observed change in band position may be due to the change in internuclear distance of Fe^{2+} and O^{2-} ions in equivalent sites.

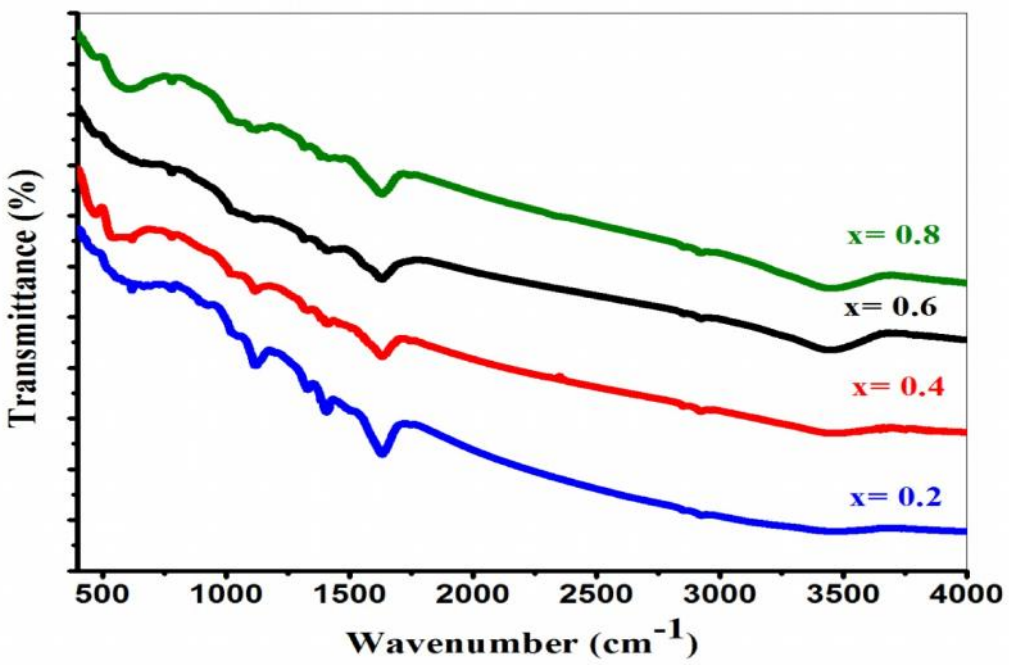

Fig.3: FTIR spectra of $Ni_xCu_{1-x}Fe_2O_4$ (x=0.2, 0.4, 0.6, 0.8) ferrite samples

3.3 SEM Study

The surface morphology of $Ni_xCu_{1-x}Fe_2O_4$ (x=0.2, 0.4, 0.6, 0.8) was analyzed by SEM and their images are shown in Fig. 4, which exhibit nearly spherical shaped grain. The small particles are loosely agglomerate and acquire spherical shapes due to magnetic nature of the samples. SEM studies reveals that particle size increases with Ni^{2+} ions concentration but the ultra fine particles are agglomerated with one another resulting in to formation of bigger particles.

International Journal of Engineering Technology Science and Research
IJETSR
www.ijetsr.com
ISSN 2394 – 3386
Volume 5, Issue 4
April 2018

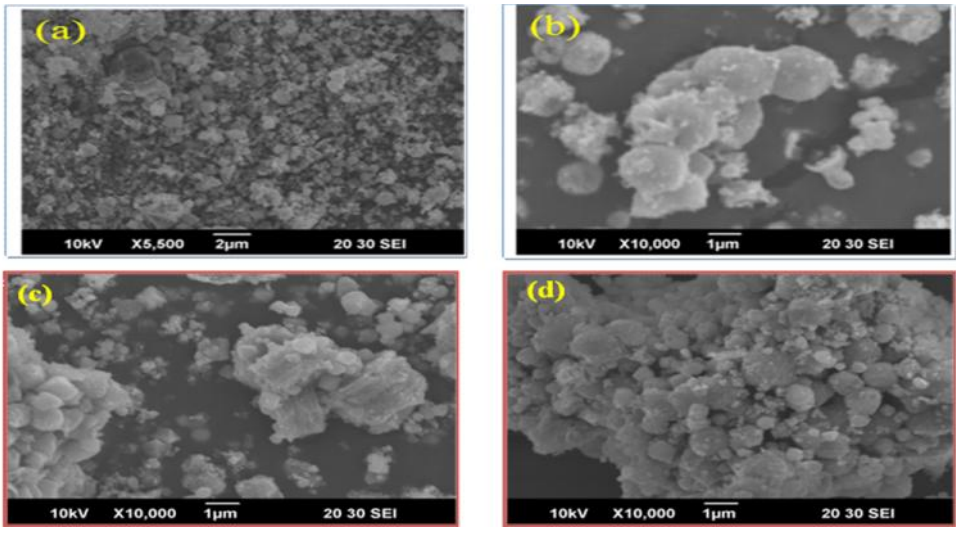

Fig.4: SEM micrographs of $Ni_xCu_{1-x}Fe_2O_4$ (a) x=0.2, (b) x=0.4, (c) x=0.6 and (d) x=0.8 samples

3.4 TEM Analysis

Transmission electron microscopy provides further insight into the morphologies and structural details of these samples. Fig. 5 shows the TEM images of $Ni_{0.2}Cu_{0.8}Fe_2O_4$, $Ni_{0.4}Cu_{0.6}Fe_2O_4$ and $Ni_{0.6}Cu_{0.4}Fe_2O_4$ samples. The observed size of ferrite nanoparticles from TEM micrographs exhibit the same trend with the size calculated using Debye-Scherer formula. TEM micrographs shows that almost all the particles are spherical in nature and have narrow particle size distribution. The particles size lie in the 10-30 nm regime. The slight agglomeration of the nanoparticles has been observed which may be due to large surface to volume ratio.

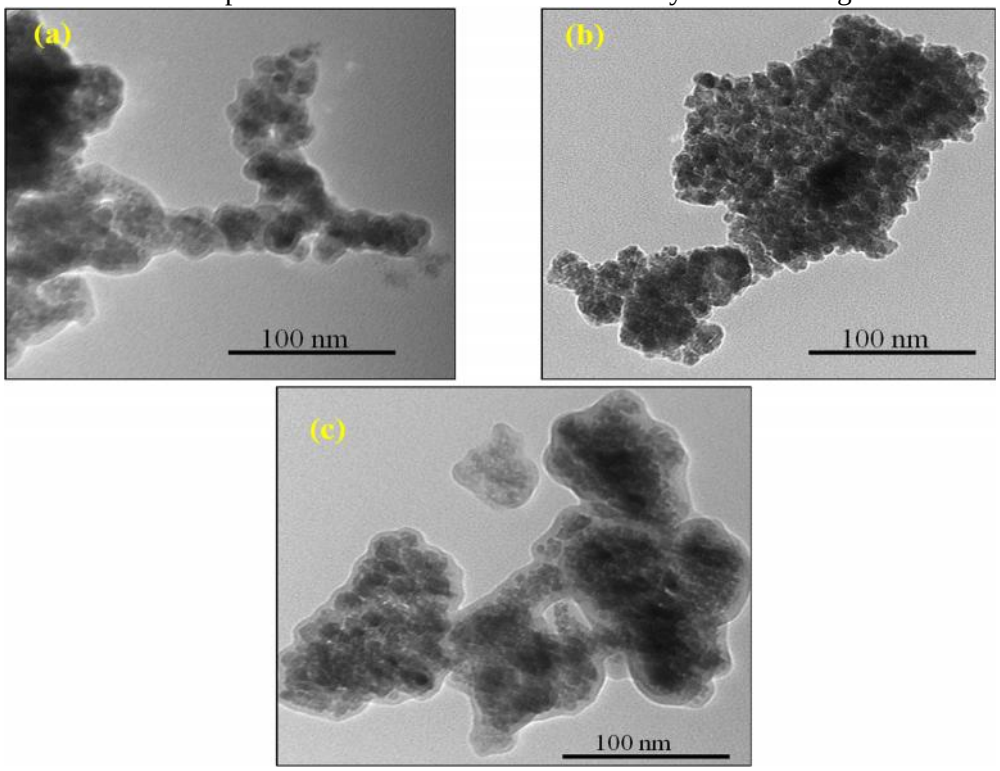

Fig.5: TEM micrographs of $Ni_xCu_{1-x}Fe_2O_4$ (a) x=0.2, (b) x=0.4 and (c) x=0.6

International Journal of Engineering Technology Science and Research
IJETSR
www.ijetsr.com
ISSN 2394 – 3386
Volume 5, Issue 4
April 2018

3.5 Magnetic measurements

Magnetic properties of the samples were measured at room temperature using a vibrating sample magnetometer. The hysteresis loops were found to be well saturated with the available applied field and are shown in Fig.6. The hysteresis loops display the characteristics of soft magnetic materials. The saturation magnetization (M_s) values of the samples are listed in Table 1. The magnetization variation with Ni content is very well in agreement with the one reported by Doh et al [19] on Ni-Cu ferrite prepared by co-precipitation method. On addition of Ni^{2+} content, the observed variation in magnetization can be explained on the basis of Neel's two sub lattice model. Accordingly A-A, B-B and A-B exchange interactions are possible. Introduction of Ni^{2+} ions at A-site, forces Fe^{3+} ions to migrate from A to the B site and hence the Fe^{3+} ions concentration increases at B site which in turn increases the magnetic moment of B sub-lattice. Consequently, on increasing Ni^{2+} content, the A-B interaction experienced by Fe^{2+} ions at B-site decreases and B-B interaction increases, resulting in spin canting [20] which in turn decreases the magnetization of B sub-lattice. Therefore, on addition of Ni^{2+} content the number of spins occupying the A sub-lattices increases causing the net magnetization to increase. In the presently prepared samples, due to the surface disorder [21] and probable modified cationic distribution, smaller magnetization is expected as compared to other synthesis methods [22].

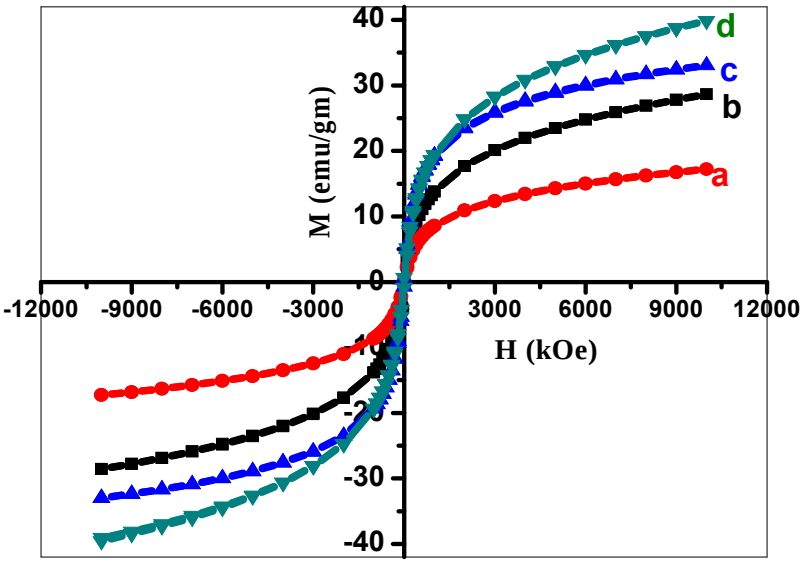

Fig.6: Hysteresis loops of $Ni_xCu_{1-x}Fe_2O_4$ samples at (a) x=0.2, (b) x=0.4, (c) x=0.6 and (d) x=0.8

4. Conclusions

The convenient and versatile sol-gel technique is used for the synthesis of mixed nickel copper nanoferrite. The XRD patterns confirm the formation of single phase cubic nickel-copper ferrite structure with reflections of the sample plane (220), (311), (400), (511) and (440). The crystallite size varies from 10 to 20nm. The lattice parameter decreases with increasing nickel content due to smaller ionic radii of nickel ions (0.69Å) as compared to copper ions (0.73Å). On substitution of nickel content in copper ferrite, the crystallite size and porosity decreases indicating that the addition of nickel has a marked effect on restricting the grain growth of spinel ferrite. From FTIR spectra it can be concluded that stretching vibration of tetrahedral metal-oxygen bond, the highest band appears in the range 600-500 (cm^{-1}) and the lowest band 450-385(cm^{-1}) is caused by metal-oxygen vibrations at octahedral sites. The characteristic peak of the tetrahedral Fe-O stretching band at 578(cm^{-1}) is present in all samples and depth decreases as the concentration of nickel increases. SEM analysis

explains that the size of samples seem to be non-uniform and agglomeration of nanoparticles. The particle size obtained from TEM micrographs are in agreement with the size as obtained from Scherer formula. The value of saturation magnetization of samples rises with increase in nickel content in $Ni_xCu_{1-x}Fe_2O_4$ samples which makes them suitable as magnetic catalyst.

Acknowledgement

Authors would like to thanks Prof. S. Annapoorni, Delhi University, Delhi for providing magnetic measurement facility.

REFERENCES

[1] Gaba S., Kumar A., Rana P. S., Arora M. 2018. Influence of La^{3+} ion doping on physical properties of magnesium nanoferrite for microwave absorption application. J. Magn. Magn. Mater. 460, 69-77.

[2] Kefeni K. K., Msagati T. A. M., and Mamba B. B. 2017. Ferrite nanoparticles: synthesis, characterization and applications in electronic device. Mater. Sci. Engg. B 215, 37-55.

[3] Ali K., Iqbal J., Jana T., Ahmad N., Ahmad I. and Wan D. 2017. Enhancement of microwaves absorption properties of $CuFe_2O_4$ magnetic nanoparticles embedded in MgO matrix. J. Alloys Compd. 696, 711–717.

[4] Sundararajan M, Sailaja V., Kennedy L. J. and Vijaya J. J. 2017. Photocatalytic degradation of rhodamine B under visible light using nanostructured zinc doped cobalt ferrite: Kinetics and mechanism. Ceram. Int. 43, 540-548.

[5] Akhtar M. N., Rahman A., Sulong A. B. and Khan M. A. 2017. Structural, spectral, dielectric and magnetic properties of nanosized ferrite for microwave absorption and high frequency applications. Ceram. Int. 43, 4357-4365.

[6] Pour S. A., Shaaterian H. R., Afradi M. and El-Ebadi A. Y. 2017. Carboxymethyl cellulose (CMC) loaded Co-Cu doped manganese ferrite nanorods as a new dual modal simultaneous contrast agent for magnetic resonance imaging and nanocarrier for drug delivery system. J. Magn. Magn. Mater. 438, 85-94.

[7] Al-Ghamdi A. A., Al-Hazmi F. S., Memes L. S., Shokr F. S. and Bronstein L. M. 2017. Evolution of the structure, magnetic and optical properties of $Ni_{1-x}Cu_xFe_2O_4$ spinel ferrites prepared by soft mechanochemical method. J. Alloys Compd. 712, 82-89.

[8] Skandan G., Hahn H., Roddy M. and Carnnon W. R. 1994. Ultrafine-Grained Dense Monoclinic and Tetragonal Zirconia. J. Am. Ceram. Soc. 77, 1706.

[9] Boobalan T., Pavithradevi S., Suriyanarayanan N., Raja M. M. and Kumar E. R. 2017. Preparation and characterization of polyol assisted ultrafine Cu-Ni-Mg-Ca mixed ferrite via co-precipitation method. J. Magn. Magn. Mater. 428, 382-389.

[10] Babu K. R., Rao K. R. and Babu B. R. 2017. Cu^{2+} - modified physical properties of cobalt-nickel ferrite. J. Magn. Magn. Mater. 434, 118-125.

[11] Das P. S. and Singh G. P. 2016. Structural, magnetic and dielectric study of Cu substituted NiZn ferrite nanorod. J. Magn. Magn. Mater. 401, 918-924.

[12] Gholizadeh A. and Jafari E. 2017. Effect of sintering atmosphere and temperature on structural and magnetic properties of Ni-Cu-Zn ferrite nano-particles: Magnetic enhancement by a reducing atmosphere. J. Magn. Magn. Mater. 422, 328-336.

[13] Yadav R. S., Kuritka I., Vilkacova J., Havlica J., Masilko J., Kalina L., Tkacz J., Enev V. and Hajduchova M. 2017. Structural, magnetic dielectric and electrical properties of $NiFe_2O_4$ spinel ferrite nanoparticles prepared by honey-mediated sol-gel combustion. J. Phys. Chem. Solids 107, 150-161.

[14] Yadav N., Kumar A., Rana P. S., Rana D. S., Arora M. and Pant R. P. 2015. Finite size effect on Sm^{3+} doped $Mn_{0.5}Zn_{0.5}Sm_xFe_{2-x}O_4$ ($0 \le x \le 0.5$) ferrite nanoparticles. Ceram. Int. 41, 8623-8629.

[15] Kumar A., Yadav N., Rana D. S., Kumar P., Arora M. and Pant R. P. 2015. Structural and Magnetic studies of the nickel doped $CoFe_2O_4$ ferrite nanoparticles ferrite synthesized by chemical co-precipitation method. J. Magn. Magn. Mater 394, 379.

[16] Kumari N., Kumar V. and Singh S. K. 2014. Effect of Cr^{3+} substitution on properties of nano- $ZnFe_2O_4$, J. Alloys Compd. 622, 628-634.

[17] Naidu V. 2011. Study of Electrical & Magnetic properties in Nanosized Ce-Gd Doped Magnesium Ferrite. Int. J. Computer Appl. 27, 0975.

[18] Yadav R. S., Havlica J., Masilko J., Kalina L., Wasserbauer J., Hajduchova M., Enev V., Kuritka I. and Kozakova Z. 2015. Effects of annealing temperature variation on the evolution of structutal and magnetic properties of $NiFe_2O_4$ nanoparticles synthesized by starch assisted sol-gel auto combustion method. J. Magn. Magn. Mater. 394, 439-447.

[19] Doh S. G., Kim E. B., Lee B. H. and Oh H. J. 2004. Characteristics and Synthesis of Cu-Ni ferrite nanopowders by co-precipitation method with ultrasound irradiation. J. Magn. Magn. Mater. 272, 2238-2240.

[20] Shirsath S. E., Toksha B. E., Kadam R. H., Patange S. M., Mane D. R., Jangam G. S. and Ghasemi A. 2010. Doping effect of Mn^{2+} on the magnetic behavior in Ni-Zn ferrite nanoparticles prepared by sol-gel auto-combustion. J. Phys. Chem. Solids 71, 1669-1675.

[21] Rashad M. M. 2007. Magnetic properties of nanocrystalline magnesium ferrite by co-precipitation assisted with ultrasound irradiation. J. Mater. Sci. 42, 5248-5255.

[22] Rao B. P., Caltun O., Cho W. S., Kim C. H. and Kim Gi C. 2007. Synthesis and Characterization of mixed ferrite nanoparticles. J. Magn. Magn. Mater. 310, 812-814.